

AperTO - Archivio Istituzionale Open Access dell'Università di Torino

Calcium signals: analysis in time and frequency domains

This is a pre print version of the following article:

Original Citation:

Availability:

This version is available <http://hdl.handle.net/2318/133521> since 2021-04-10T11:18:24Z

Published version:

DOI:10.1016/j.jneumeth.2011.05.009

Terms of use:

Open Access

Anyone can freely access the full text of works made available as "Open Access". Works made available under a Creative Commons license can be used according to the terms and conditions of said license. Use of all other works requires consent of the right holder (author or publisher) if not exempted from copyright protection by the applicable law.

(Article begins on next page)

Calcium signals: analysis in time and frequency domains

F. A. Ruffinatti^a, D. Lovisolò^{a,d,e}, C. Distasi^{b,e}, P. Ariano^{f,d}, J. Erriquerz^b,
M. Ferraro^{c,e}

^a*Università di Torino, Dipartimento di Biologia Animale e dell'Uomo, Torino, Italy*

^b*Università del Piemonte Orientale, Dipartimento di Scienze Chimiche, Alimentari,
Farmaceutiche e Farmacologiche, Novara, Italy*

^c*Università di Torino, Dipartimento di Fisica Sperimentale, Via P. Giuria 1, 10125
Torino, Italy*

^d*NIS, Centre of Excellence for Nanostructured Interfaces and Surfaces, University of
Turin, Italy*

^e*NIT, Neuroscience Institute of Turin, Italy*

^f*IIT, Center for Space Human Robotics, Italian Institute of Technology, Polytechnic
University of Turin, Italy*

Abstract

Cytosolic calcium signals play important roles in processes such as cell growth and motility, synaptic communication and formation of neural circuitry. These signals have complex time courses and their quantitative analysis is not easily accomplished; in particular it may be difficult to evidence subtle differences in their temporal patterns. In this paper, we use wavelet analysis to extract information on the structure of $[Ca^{2+}]_c$ oscillations. To this aim we have derived a set of indices by which different $[Ca^{2+}]_c$ oscillatory patterns and their change in time can be extracted and quantitatively evaluated. This approach has been validated with examples of experimental recordings showing changes in oscillatory behavior in cells stimulated with a calcium-releasing agonist.

Keywords:

computational methods, wavelet analysis, calcium signals

Email addresses: federicoalessandro.ruffinatti@unito.it (F. A. Ruffinatti),
davide.lovisolo@unito.it (D. Lovisolò), carla.distasi@pharm.unipmn.it (C.
Distasi), paolo.ariano@gmail.com (P. Ariano), jessica.erriquerz@pharm.unipmn.it
(J. Erriquerz), ferraro@ph.unito.it (M. Ferraro)

1. Introduction

A large array of cellular functions is under the control of fine and complex changes in the free cytosolic calcium concentration, $[Ca^{2+}]_c$. These changes convey information on the specific status of the metabolic machinery and on the signals impinging on the cell itself, and this information can be coded both in amplitude and frequency (Oike et al., 1994; Prank et al., 2000). Additionally, these intracellular events are usually compartmentalized, i.e. they are restricted to specific subcellular domains, with different compartments showing different patterns of Ca^{2+} signalling (Frey et al., 2000; Goldberg and Yuste, 2005; Raymond and Redman, 2006). In nerve cells, the role of these intracellular signals is of particular relevance: they can regulate a wide set of processes, from cell to cell communication to integration of information at the cell body and to transcriptional events. Moreover, they have specific roles at defined developmental stages, such as in the growth, orientation and stabilization of neuronal processes (dendrites and axons) and in the correct formation of neuronal circuitry (Wen and Zheng, 2006).

The generation of these cytosolic signals, usually showing an oscillatory pattern, is the result of a convergent and tightly regulated set of activations and deactivations of calcium import and export mechanisms, together with pathways involving exchange of the ion between the cytosol and intracellular compartments (Uhlén and Fritz, 2010). The resulting responses are often of complex time course, and their quantitative analysis is not so obvious. In many cases, they appear to be non-periodic and it may be difficult to evidence subtle differences in signal patterns by qualitative or semiquantitative observation. On the other hand, evidencing statistical differences may be necessary when analyzing changes in activity following treatments with different agonists (neurotransmitters, hormones, growth factors, guidance molecules) or comparing activity in different subcellular domains (soma, growth cone, etc.). Some simple and in some cases effective approaches have been developed (Constantin et al., 2009), but, in general, spectral analysis is mandatory. Fourier transform has been widely used (see e.g. Uhlén, 2004); however, it provides a mean of analysis solely in the space of frequencies. To overcome this limitation, some authors have employed wavelet analysis (Gorbunova and Spitzer, 2002; Suzuki et al., 2002; Wegner et al., 2006), that takes into account the local frequency composition of the signal and enables the signal to be analyzed both in frequency and time spaces. On the other hand, many applications of wavelet analysis do not provide quantitative param-

38 ters to describe changes in the frequency composition of oscillatory patterns
39 following stimulation protocols. This is a relevant issue, since such changes
40 may provide relevant information on the kinetics of the mechanisms involved.

41 In this paper, we introduce a more sophisticated approach to wavelet
42 analysis, and show that it can be of significant help in extracting informa-
43 tion from traces in which changes in the pattern of Ca^{2+} oscillations cannot
44 be evidenced by qualitative observation. To this purpose, starting from the
45 standard wavelet analysis, we have derived a set of indices by which differ-
46 ent $[\text{Ca}^{2+}]_c$ oscillatory patterns and their change in time can be extract and
47 quantitatively evaluated. The potential usefulness of this approach can be
48 extended to other contexts, such as the analysis of differences between activ-
49 ities in subcellular domains of the same neuron, and, more generally, of the
50 same cell.

51 **2. Mathematical preliminaries**

52 A standard method to analyze a signal $f(t)$ is via its Fourier transform
53 which, however, provides information only on the frequencies making up the
54 signal: that is to say that although, in principle, it is possible to determine
55 all the frequencies present in a signal, the time at which they occur cannot be
56 determined. To overcome this problem in the past decades several solutions
57 have been developed to represent a signal in the time and frequency domain
58 at the same time.

59 A typical example is the windowed Fourier transform where the kernel
60 of the Fourier transform is multiplied by a temporal window, say $g_a(t - b)$,
61 where the parameter a measures the width of the window, and the parameter
62 b is used to translate the window over the whole time domain. The result-
63 ing transform is called the Gabor transform (windowed Fourier transform)
64 (Lokenath, 1998).

65 The width of the window, determined by a , provides a trade-off between
66 frequency and time resolution: large windows (i.e. large a) give high resolu-
67 tion of frequency and low time resolution, whereas narrow windows improve
68 time resolution but provide a less accurate frequency representation. In other
69 words a small a gives accurate information on the time course of the signal
70 but it may lead to a coarse frequency representation, possibly losing relevant
71 information on the structure of the signal itself; conversely, a large a provides
72 an accurate representation of the signal structure but important events in the
73 time course of the signal may be overlooked.

74 The problem of achieving good time resolution for the high frequency
75 transients and good frequency resolution for low frequency components can
76 be solved with the use of wavelets, a family of functions constructed from
77 translations and dilations of a single function called the “mother wavelet” ψ
78 (for a clear historical introduction see Lokenath (1998) and, for an in depth
79 treatment, Daubechies (1992) and Mallat (1999): the literature on wavelet is
80 virtually unlimited). This function must satisfy certain technical conditions
81 (see, for instance, Antonini et al., 1992), among which $\int \psi(t) dt = 0$, so that
82 ψ must exhibit some oscillations and a rapidly decreasing trend. The set of
83 wavelets is obtained by the formula

$$\psi^{(a,b)}(t) = \frac{1}{|a|^{1/2}} \psi\left(\frac{t-b}{a}\right), \quad (1)$$

84 where a is a scaling parameter which measures the degree of compression
85 or scale, and b a translation parameter which determines the time location
86 of the wavelet (Daubechies, 1992). If $|a| < 1$ the wavelet $\psi^{(a,b)}$ corresponds
87 mainly to higher frequencies, when $|a| > 1$ it has a larger time-width than
88 ψ and corresponds to lower frequencies. In other words on a large scale, the
89 resolution is coarse in the time domain and fine in the frequency domain
90 and, as the scale parameter a decreases, the resolution in the time domain
91 becomes finer, while that in the frequency domain becomes coarser. Thus,
92 wavelets have time-widths adapted to their frequencies and this is the main
93 reason for their success in time-frequency analysis.

94 Functions $\psi^{(a,b)}$ form the kernel of the wavelet transform:

$$W^{(a,b)} = \frac{1}{|a|^{1/2}} \int_{-\infty}^{+\infty} \psi^*\left(\frac{t-b}{a}\right) f(t) dt, \quad (2)$$

95 where $*$ denotes complex conjugation.

96 Here we have chosen the Morlet function as mother wavelet (Goupillaud
97 et al., 1984):

$$\psi(t) = \frac{c_s}{\pi^{1/4}} \exp\left(-\frac{1}{2}t^2\right) [\exp(ist) - k_s], \quad (3)$$

98 where $k_s = \exp(-\frac{1}{2}s^2)$ and $c_s = [1 + \exp(-s^2) - 2\exp(-\frac{3}{4}s^2)]^{-1/2}$ is the
99 normalization constant. Usually the parameter s is taken to be equal or
100 larger than 5, so that $k_s \simeq 0$ and $c_s \simeq 1$: (3) becomes

$$\psi(t) \simeq \frac{1}{\pi^{1/4}} \exp\left(-\frac{1}{2}t^2\right) \exp(ist) \quad (4)$$

and the corresponding graph is shown in Fig. 1.

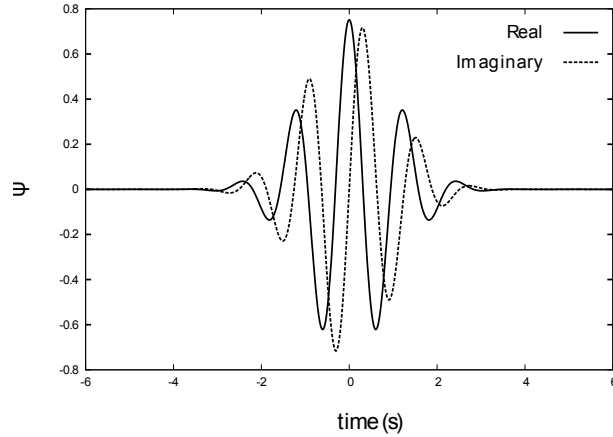


Figure 1: Real and imaginary parts of the Morlet mother wavelet, as given by Eq. (4).

101
102

The wavelets transform is

$$\begin{aligned}
 W^{(a,b)} &= \frac{1}{|a|^{1/2}} \int_{-\infty}^{+\infty} \psi^* \left(\frac{t-b}{a} \right) f(t) dt \\
 &= \frac{1}{(\pi a^2)^{1/4}} \int_{-\infty}^{+\infty} \exp \left[-\frac{1}{2} \left(\frac{t-b}{a} \right)^2 \right] \exp \left[-i \frac{s}{a} (t-b) \right] f(t) dt,
 \end{aligned} \tag{5}$$

103 where we have used $s = 5$. It should be noted that b is a time variable
 104 and that s/a is related to the distance T_p between successive peaks of the
 105 mother wavelet (see Fig. 1) by the relation $s/a = 2\pi/T_p$ so that it is possible
 106 to define a frequency of the wavelet by the relation $\nu = s/2\pi a$ (Goupillaud
 107 et al., 1984; Mallat, 1999). Thus, in the following the wavelet transform will
 108 be denoted by $W(t, \nu)$: the amplitude (modulus) of W defines the *scalogram*,
 109 a graphical representation of the signal in the time-frequency domain.

110 3. Analytical methods

111 In this section a method of analysis will be described using recordings of
 112 changes in the intracellular free calcium concentration from cultured chick cili-
 113 ary ganglion (CG) glial cells. The signals represent responses to application
 114 to the extracellular solution of the agonist nicotinic acid adenine dinucleotide

115 phosphate (NAADP), a molecule that activates calcium release from intra-
116 cellular stores (Genazzani and Billington, 2002) and that can exert its action
117 when extracellularly applied (Billington et al., 2006). Changes in $[Ca^{2+}]_c$
118 have been recorded by means of the fluorescent calcium indicator Fura-2.
119 More details on the experimental procedures will be given in Section 3.4.

120 A graphical representation of the wavelet transform of one of such signals
121 $f(t)$ is presented in Fig. 2. The signal itself is in the upper box of the figure,
122 and the modulus (amplitude) $|W(t, \nu)|$ of its wavelet transform is displayed
123 in the lower box using an appropriate pseudocolor look-up table. It is known
124 that wavelet transforms in finite time intervals give rise to the so called
125 cone of influence at the edges of the time span of the recording (Torrence
126 and Compo, 1998); here a detrending procedure was used that, ensuring a
127 matching between the start and the end of the signal, can reduce the cone
128 of influence artifact, by removing edge discontinuity; however this procedure
129 does nothing about the most important source of this effect, namely the lack
130 of information on the events occurring before the start and after the end of
131 the recording.

132 This trace was selected since even from a qualitative observation it can
133 be concluded that it shows a sharp response to the agonist, in the form of a
134 transient oscillatory burst. From the figure it is apparent that $|W(t, \nu)|$ takes
135 its maximum values during the oscillatory burst of $f(t)$, and that outside the
136 areas of these peaks its values are relatively small, except for a low frequency
137 component that corresponds to an overall oscillation of $f(t)$. Furthermore,
138 it can be noted that peaks are more spread out at low frequencies, as ex-
139 pected from wavelet theory: at low frequency the time resolution tends to
140 be less precise (Mallat, 1999). Thus the use of wavelet analysis implies some
141 uncertainty in time (i.e. the exact time at which a specific component can
142 be localized) and this holds mainly for low frequency components. However,
143 the extent of the oscillatory burst is in good agreement with the temporal
144 position of the peaks in the scalogram, thus showing that wavelets provide
145 temporal information about the start and duration of the oscillatory part of
146 the signal.

147 While $|W(t, \nu)|$ provides information on both the oscillatory structure of
148 the signal and its temporal trend, the question remains of how this infor-
149 mation can be used. In many applications requiring to discriminate among
150 different experimental conditions, e.g. in order to obtain quantitative indices
151 of the effect of a particular stimulus on the time course of the signal, it may
152 be useful to focus on time varying measures obtained by integration on the

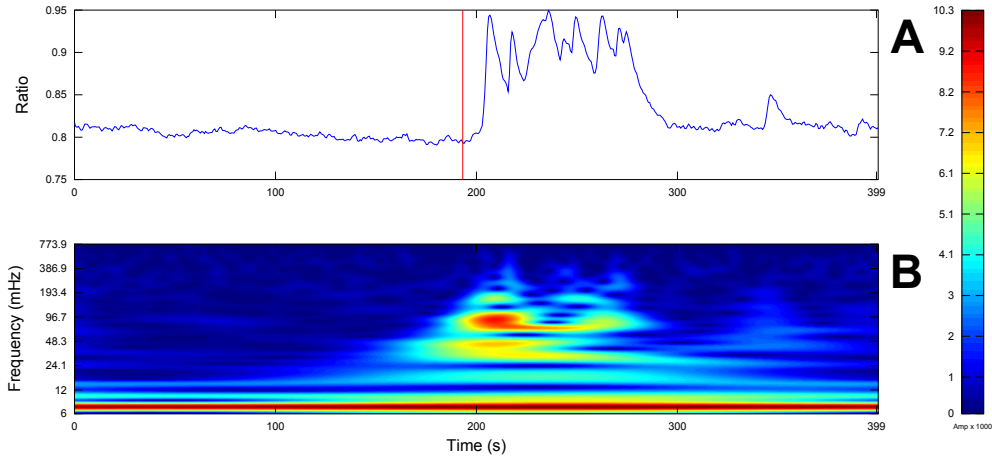


Figure 2: **A**: oscillations in $[Ca^{2+}]_c$ observed in response to stimulation of a chick CG glial cells with 10 nM NAADP. A vertical line marks the starting time of perfusion with the agonist. **B**: $|W(t, \nu)|$: amplitude of the wavelet transform as a function of time and frequency.

153 frequency line, or, conversely, measures that depend solely on the frequencies
 154 making up the signal.

155 In Fig. 3 the upper and left insets represent the result of the integration
 156 of $|W(t, \nu)|^2$ along frequency and time respectively. In other words the top
 157 of the figure displays the so called energy density $E(t)$ (Bussow, 2007)

$$E(t) = \int |W(t, \nu)|^2 d\nu, \quad (6)$$

158 in which all contributions of all frequencies are integrated to provide a func-
 159 tion of time. Note that $E(t)$ starts increasing before the application of the
 160 stimulus: this is an effect of the spreading of the maxima at low frequencies,
 161 remarked before. On the left the power spectrum is represented:

$$P(\nu) = \int |W(t, \nu)|^2 dt. \quad (7)$$

162

163 Note that this power spectrum is similar, but not the same, to the one
 164 obtained with a Fourier transform; a comparison is shown in Fig. 4.

165 In the next sections methods will be presented to compute differences
 166 between signals obtained in different experimental conditions, by making use
 167 of appropriate indices in time and frequency spaces, respectively.

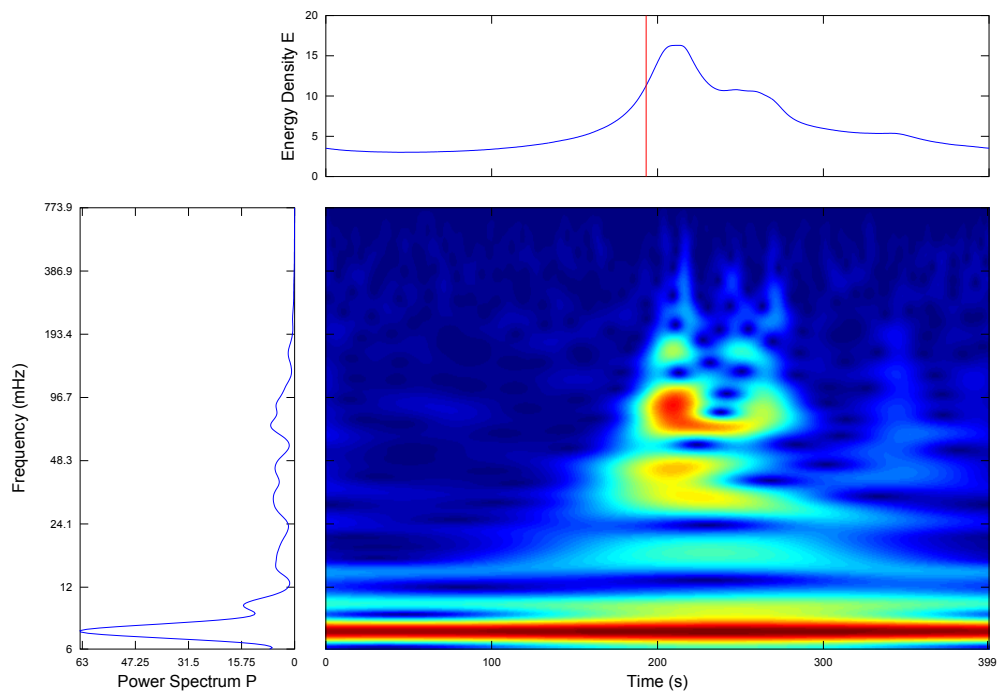


Figure 3: Projections. The central box shows the modulus of the wavelet transform. In the insets: on the left the power spectrum as defined in Eq. (7) and on the top the energy density (see Eq. (6)).

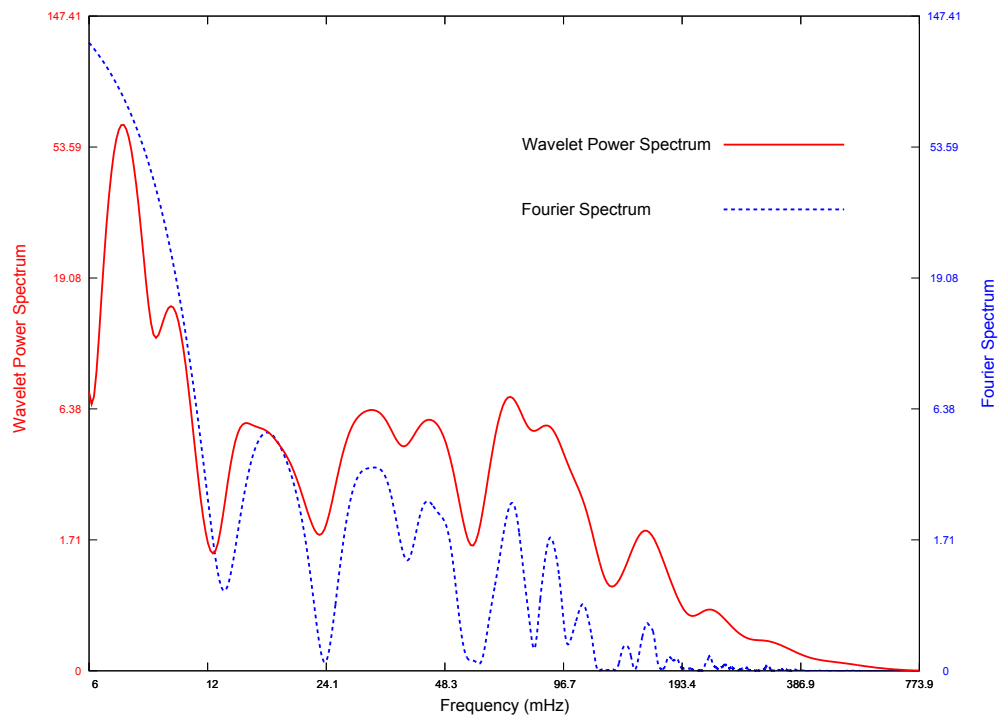


Figure 4: Fourier and wavelet spectra superimposed in a log-log coordinates: the wavelet power spectrum results in a smoother version of the Fourier spectrum, overemphasizing high frequencies.

168 *3.1. Focusing on time*

169 In most cases of interest the main contributions to energy density, at each
 170 time point, are concentrated around a few maxima (see Fig. 2), that arise
 171 precisely in correspondence with the most relevant events in the signal such
 172 as sharp peaks or oscillatory bursts, and these events are characterized by
 173 the occurrence of relatively high frequency components.

174 In order to discriminate between results obtained in different experimental
 175 conditions a suitable representation of the signal must take into account both
 176 aspects. This can be done, for instance, by summing the contributions of the
 177 maxima of $|W(t, \nu)|$ along the ν axis, weighted by the corresponding values
 178 of ν . Maxima of $|W(t, \nu)|$ along the frequency axis can be obtained by the
 179 conditions

$$\begin{cases} \frac{\partial}{\partial \nu} |W| & = 0 \\ \frac{\partial^2}{\partial \nu^2} |W| & < 0 \end{cases}, \quad (8)$$

180 and a new index J of energy density can be defined as

$$J(t) = \frac{1}{2\epsilon} \int_{t-\epsilon}^{t+\epsilon} \sum_{i=1}^{n(\tau)} |W(\tau, \nu_i)|^2 \nu_i(\tau) d\tau, \quad (9)$$

181 where $\{\nu_i(\tau)\}$ is exactly the set of directional local maxima of W along the
 182 ν axis, at time τ . Since the number of these maxima changes in time, the
 183 parameter n is expressed as a function of τ . Integration simply serves to
 184 regularize the index, by avoiding abrupt variations due to discontinuities of
 185 frequency paths. The index J , calculated using the signal of Fig. 2, is shown
 in Fig. 5.

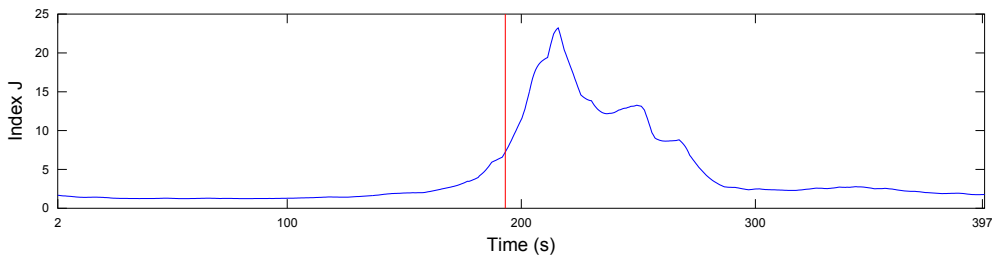


Figure 5: Time course of the index J , computed applying Eq. (9) to the modulus of the wavelet transform shown in Fig. 2.

186

187 The index J gives a good quantitative evaluation of the effect of the
 188 agonist on the oscillatory activity shown in Fig. 2; the initial peak reflects
 189 the greater amplitude of the oscillations in the first part of the burst.

190 A comparison with E (compare with the inset in Fig. 3) shows that J
 191 provides a representation that discriminates better between pre- and post-
 192 stimulus activity: in particular the maximum is sharper and J starts increas-
 193 ing after the application of the stimulus. This is because the index J has
 194 been obtained by taking into account the peaks of the amplitudes weighted by
 195 the frequencies, so that higher frequency components have a greater weight.
 196 Since high frequencies are better localized in time, this approach provides a
 197 reduction of the effect due to the spreading at low frequencies; in other words
 198 it enhances the components better resolved in time minimizing the effects of
 199 delocalization at low frequencies. The obvious trade-off is that low frequen-
 200 cies are somehow underrepresented; however, this is not a serious flaw since,
 201 as stated above, low frequencies correspond just to a global oscillatory trend
 202 of the signal.

203 A global measure can be derived simply by taking the time average of J ,

$$\bar{J} = \frac{1}{\delta t} \int_{t_i}^{t_f} J(t) dt, \quad (10)$$

204 where $\delta t = t_f - t_i$ is the duration of the signal.

205 Suppose we are given two signals f_1 and f_2 , then the corresponding indices
 206 \bar{J}_1 and \bar{J}_2 can be used to derive a measure of the difference in the oscillatory
 207 components, for instance by defining

$$r_J = \frac{\bar{J}_2}{\bar{J}_1}. \quad (11)$$

208 Thus r_J is a measure of the activity variation of the whole trace: $r_J > 1$
 209 stands for an enhancement, while $0 < r_J < 1$ corresponds to a decrease (note
 210 that since $J(t)$ is a positive defined value, r_J too is always positive).

211 As an example consider again the signal of Fig. 2 and let δt_1 , δt_2 be
 212 the intervals before and after the application of the stimulus, respectively.
 213 Then \bar{J}_1 , \bar{J}_2 are the temporal averages of J before and after the stimulus,
 214 and their values are $\bar{J}_1 = 1.86$, $\bar{J}_2 = 6.74$. The ratio $r_J = 3.63$ is relatively
 215 large, showing that \bar{J}_1 , \bar{J}_2 are able to provide a measure of the effect of the
 216 stimulus on the signal time course; by comparison note that the ratio of pre-
 217 and post-stimulus averages of the density of energy $E(t)$ is just 1.89.

218 In conclusion, by means of the index $J(t)$, we can obtain an instantaneous
 219 estimate of the oscillatory activity of the signal and by computing its tem-
 220 poral mean \bar{J} , we can assign a single scalar value to each arbitrarily defined
 221 temporal interval (for instance a pre-treatment value \bar{J}_1 and a post-treatment
 222 value \bar{J}_2). Finally, the ratio r_J between \bar{J}_2 and \bar{J}_1 is a global measure of the
 223 variation of the oscillatory trend within a single trace; since it is defined as
 224 a ratio between two temporal mean quantities, any basal component can be
 225 ignored.

226 3.2. Focusing on frequencies

227 Consider the time average, in an interval δt , of the modulus $|W(t, \nu)|$ of
 228 the wavelet transform:

$$\mathbf{V}(\nu) = \frac{1}{\delta t} \int_{t_i}^{t_f} |W(t, \nu)| dt. \quad (12)$$

229 This average is a function of ν that can be considered to be represen-
 230 tative of the frequency spectrum within the interval. Note also that \mathbf{V} can
 231 be regarded as an infinite-dimensional vector, whose components are the fre-
 232 quencies ν , and component values are given by $\mathbf{V}(\nu)$; therefore some tools of
 233 vector analysis can be applied here. For instance it is possible to determine
 234 a distance d , in the frequency space, between signals recorded in different
 235 experimental conditions.

236 Consider two signals f_1, f_2 of duration $\delta t_1, \delta t_2$ respectively, and the cor-
 237 responding vectors $\mathbf{V}_1(\nu)$ and $\mathbf{V}_2(\nu)$. The distance d is defined as

$$d = \left[\int_0^{+\infty} [\mathbf{V}_2(\nu) - \mathbf{V}_1(\nu)]^2 d\nu \right]^{1/2}, \quad (13)$$

238 and it is straightforward to show that

$$d = [\|\mathbf{V}_1\|^2 + \|\mathbf{V}_2\|^2 - 2\|\mathbf{V}_1\|\|\mathbf{V}_2\|\cos\theta]^{1/2}, \quad (14)$$

239 where

$$\|\mathbf{V}\| = \left[\int_0^{+\infty} [\mathbf{V}(\nu)]^2 d\nu \right]^{1/2}, \quad (15)$$

240 is the norm of $\mathbf{V}(\nu)$, and

$$\cos\theta = \frac{1}{\|\mathbf{V}_1\|\|\mathbf{V}_2\|} \int_0^{+\infty} \mathbf{V}_1(\nu) \cdot \mathbf{V}_2(\nu) d\nu. \quad (16)$$

241 Equation (14) can be rewritten as

$$d = [\Delta^2 + 2 \|\mathbf{V}_1\| \|\mathbf{V}_2\| (1 - \cos \theta)]^{1/2}, \quad (17)$$

242 where Δ is the modulus of the difference between the norms, namely $\Delta =$
243 $\left| \|\mathbf{V}_1\| - \|\mathbf{V}_2\| \right|$.

244 In practice integrals (13), (15) and (16) must be replaced by summations
245 over a discrete and finite set of frequencies, ranging from $\nu_{low} = \frac{1}{T}$ to Nyquist
246 frequency $\nu_{nyq} = \frac{1}{2\delta\tau}$, where T is the total recording time, while $\delta\tau$ is the
247 sampling time.

248 In reference to equation (17), the distance d depends on two factors:
249 the difference Δ between the norms of vectors \mathbf{V}_1 and \mathbf{V}_2 and their relative
250 orientations. Consider the case $\theta = 0$: the vectors are parallel (in the infinite-
251 dimensional space), that is to say that they have the same frequency content,
252 the only difference being a scale factor. In this case $d = \Delta$. Conversely if
253 $\theta = \pi/2$ the scalar product is zero, that is $\mathbf{V}_1, \mathbf{V}_2$ are orthogonal and that
254 means that one signal is made up of frequencies that have zero amplitude in
255 the other one. Now $d = [\|\mathbf{V}_1\|^2 + \|\mathbf{V}_2\|^2]^{1/2}$.

256 However, some care must be taken when considering the distance d . For
257 instance, if $\|\mathbf{V}_1\|$ and $\|\mathbf{V}_2\|$ are equal ($\Delta = 0$) and very large even a small
258 angular difference θ can lead to a large distance d . Thus, in this framework,
259 it is appropriate to consider together with d and Δ the angular difference θ ,
260 that does not depend on the norms.

261 An example is shown in Fig. 6. As before $\delta t_1, \delta t_2$ are the pre- and post-
262 stimulus time intervals and \mathbf{V}_1 and \mathbf{V}_2 are the corresponding vectors. It is
263 apparent from Fig. 6 that the difference between vectors \mathbf{V}_1 and \mathbf{V}_2 is due
264 to both factors: \mathbf{V}_2 is larger than \mathbf{V}_1 at all frequencies, and at intermediate
265 frequencies it has peaks that do not appear in \mathbf{V}_1 : here $d = 3.43$, $\Delta = 2.11$,
266 that is Δ contributes to the 60% of the distance d .

267 This approach can unravel subtle differences in the spectral components
268 of the signal in different experimental conditions, that may reflect different
269 mechanisms of generation of calcium oscillations.

270 3.3. Computational considerations

271 In order to carry out the analysis a software, called KYM, has been devel-
272 oped under the freely redistributable GNU Octave environment (Eaton et al.,
273 2008). Octave is a high-level language, primarily intended for numerical com-
274 putations. It provides a convenient command line interface for solving linear

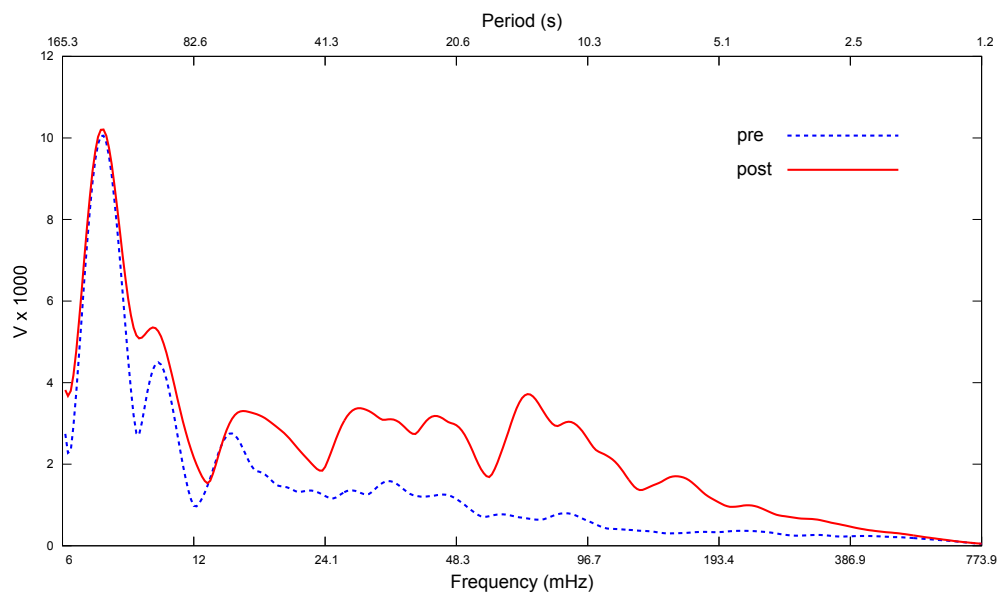


Figure 6: Vector analysis. The dashed line represents the vector \mathbf{V}_1 , computed from the pre-stimulus signal, whereas the continuous line refers to \mathbf{V}_2 , corresponding to the post-stimulus signal.

275 and nonlinear problems numerically, and for performing other numerical ex-
276 periments using a language that is mostly compatible with other popular
277 high-level language environments. As it is easily expandable and customiz-
278 able we wrote KYM as user-defined functions in Octave's 3.2.3 own language
279 and tested it on both Microsoft and Linux Debian systems.

280 At the present KYM is made up of 14 .m files each containing a single
281 function, for a total of about 1700 code lines, but only 4 of them (VX, WT,
282 PD, FEAT) need to be directly managed by the end user. The other ones
283 are auxiliary functions invoked on the fly by the mains. All numerical and
284 graphic results presented in this work have been obtained by means of KYM
285 routines but only a small part of the features is shown in the present work.
286 The architecture allows component reuse and quick prototyping of new tracks
287 processing algorithms, making new developments and further optimizations
288 easier to be implemented. KYM has a command-line user-interaction that
289 has not been developed taking into account the end users and, therefore, a
290 future effort will be to make a user-friendly interface.

291 In order to use KYM, data need to be stored in a .csv (comma separated
292 values) file. It must contain the vector of time samples as first column, while
293 the time courses of the fluorescence intensity for each cell (or region of in-
294 terest) must fill the next columns in the matrix. Some parameters can be
295 passed as argument to the main functions, in order to specify time units,
296 points at which changes in the extracellular medium have been performed,
297 threshold levels, and so on. Actual wavelet computation consists in the usual
298 method that implements a time convolution as a product in the Fourier
299 transformed domain; code for this algorithm can be downloaded at <http://www-stat.stanford.edu/~wavelab/>. Peak detection uses a technique
300 that is based on images dilation (see for instance <http://www.mathworks.com/matlabcentral/fileexchange/authors/26510/>). The rest of code has
301 been written and developed ad hoc to perform the analysis presented here.
302 At the moment KYM does not implement any algorithm to detect the cone
303 of influence; this problem will be addressed in an upgraded version of the
304 software.
305

307 We make KYM available as supplementary material: as it is an open
308 source code one can inspect it to see exactly what algorithms have been
309 used, and then modify the source to produce a better code or to satisfy other
310 particular needs. Users may redistribute it and/or modify it under the terms
311 of the GNU General Public License (GPL) as published by the Free Software
312 Foundation. Because KYM is a free software users are encouraged to help

313 make Octave more useful by writing and contributing additional functions
314 for it, and by reporting any problems they may have.

315 The most up-to-date version can be downloaded from the well-established
316 public-domain repository SourceForge ([http://sourceforge.net/projects/
317 kym/](http://sourceforge.net/projects/kym/)). The .m files come with an extended documentation in the heading,
318 explaining the syntax and the meaning of each function and related argu-
319 ments.

320 To our knowledge this is the first open source tool specifically dedicated to
321 the analysis of the time course of cellular calcium signals and more generally
322 of oscillatory signals recorded by means of fluorescent dyes from biological
323 systems.

324 *3.4. Experimental procedures*

325 Chick ciliary ganglion cells were obtained from 7 day embryos and main-
326 tained for 1-3 days in a chemically defined N2 medium as previously described
327 (Distasi et al., 1998). Cells were loaded for 30 min at 37 °C with 0.5 μ M
328 Fura-2 (Invitrogen, USA), transferred in a perfusion chamber (Bioptechs,
329 USA) and mounted on an inverted microscope (Eclipse TE 300, Nikon,
330 Japan). Experiments were performed at a temperature of 37 °C. During
331 experiments cells were continuously superfused by means of a gravity mi-
332 croperfusion system combined with electrovalves to allow switching between
333 different solutions. The control solution was a standard Tyrode solution of
334 the following composition, in mM: NaCl, 154; KCl, 4; CaCl₂, 42; MgCl₂, 1;
335 N-(2-Hydroxyethyl)-piperazine-N'-ethanesulfonic acid (HEPES), 54; glucose,
336 5.5; NaOH to pH 7.4. $[Ca^{2+}]_c$ measurements were performed exciting the
337 dye Fura-2 alternatively at 340 nm and 380 nm for 100 ms by means of a
338 monochromator (Polychrome IV, T.I.L.L. Photonics GmbH, Germany), and
339 recording emission at 510 nm. Images were acquired with a cooled CCD
340 camera (SensiCam, PCO, Germany) and stored on a computer. Fluores-
341 cence was determined from regions of interest (ROI) covering single glial cell
342 bodies. The use of a ratiometric probe allowed to rule out any effect on
343 signal amplitudes of dye loading and potential changes in fluorescence emis-
344 sion during the experiments. Dye excitation, image acquisitions and ROI
345 analysis protocols were performed with Axon Imaging Workbench software
346 (Axon Instruments, USA). Satellite glial cells were identified on morpholog-
347 ical and functional criteria as previously reported (Bernascone et al., 2010)
348 and NAADP was synthesized and purified as described in Billington and
349 Genazzani (2000).

350 4. Results

351 The approach described above was tested on a group of traces obtained
352 from the same experiment of the trace shown in Fig. 2 (i.e. ciliary ganglion
353 glial cells challenged with 10 nM NAADP). We selected traces showing dif-
354 ferent patterns in time and for which in some cases the interpretation of the
355 results was not straightforward.

356 The upper box of Fig. 7 refers to a case in which the occurrence of a
357 change in the oscillatory pattern after the stimulus can be deduced from a
358 visual observation. The index J (middle box) starts to increase with the ap-
359 plication of the agonist, the corresponding ratio r_J has a relatively high value,
360 $r_J = 2.43$. Vector analysis (lower box) shows an increase of all frequency
361 components between 10 and 96 mHz, and indeed the distance is mainly due
362 to differences between the norms Δ since amplitude enhancement affects all
363 frequency components: $d = 2.86$ and $\Delta = 2.33$.

364 On the contrary the trace displayed in the upper box of Fig. 8 shows
365 oscillatory activity both before and after the stimulus with a random compo-
366 nent, and it is therefore difficult to extract information, by means of direct
367 observation, on the occurrence of a response. However, the relatively large
368 values taken by the index J , with $r_J = 1.64$, points to an enhancement of
369 the oscillatory pattern; vector analysis reveals that the growth of J is due
370 to a different modulation in the post-stimulus interval and in particular to
371 an increase of the components in the frequency range 24 – 98 mHz. The
372 fact that most of the distance d between \mathbf{V}_2 and \mathbf{V}_1 is due to the variation
373 of spectral contents in the pre- and post-stimulus intervals is shown by the
374 small contribution of $\Delta = 0.51$ to $d = 1.61$.

375 In the trace of Fig. 9 after the administration of the agonist a clear re-
376 sponse can be observed, consisting of a sharp transient of $[\text{Ca}^{2+}]_c$ followed
377 by a plateau with limited oscillations. The wavelet transform of this type of
378 signal is mainly formed by the contribution of a low frequency component
379 that, as explained earlier, is poorly discriminated in time; thus is not sur-
380 prising that the index J starts to slowly increase before the stimulation, and
381 it is characterized by a lower value of ratio r_J ($r_J = 1.28$). Note that the
382 step size increase in the signal produces large values of \mathbf{V}_1 and \mathbf{V}_2 that, in
383 turn, give rise to a relatively large distance ($d = 2.97$) even in absence of a
384 significant difference between the spectral content of vectors \mathbf{V}_1 and \mathbf{V}_2 , as
385 explained before. Indeed both the norm and angular differences are small:
386 $\Delta = 0.79$, $\theta = 0.24$ rad.

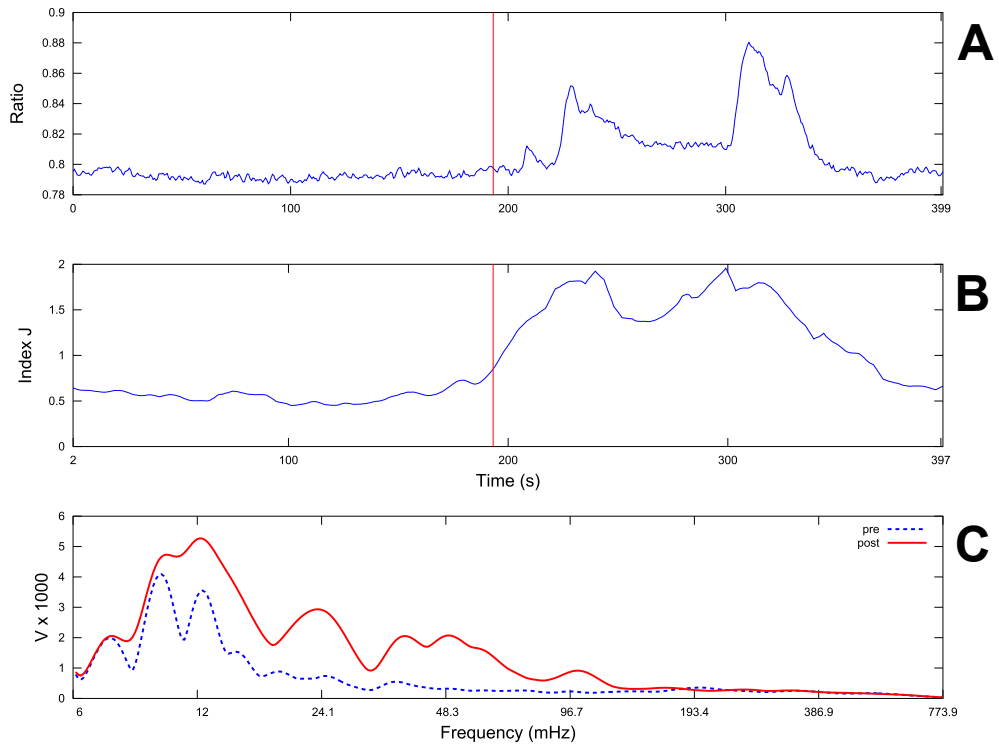


Figure 7: Second trace. **A:** oscillations in $[Ca^{2+}]_c$ observed in response to stimulation of a CG glial cells with 10 nM NAADP. **B:** time course of the index J . **C:** the dashed line represents the vector \mathbf{V}_1 , computed from the pre-stimulus signal, whereas the continuous line refers to \mathbf{V}_2 , corresponding to the post-stimulus signal.

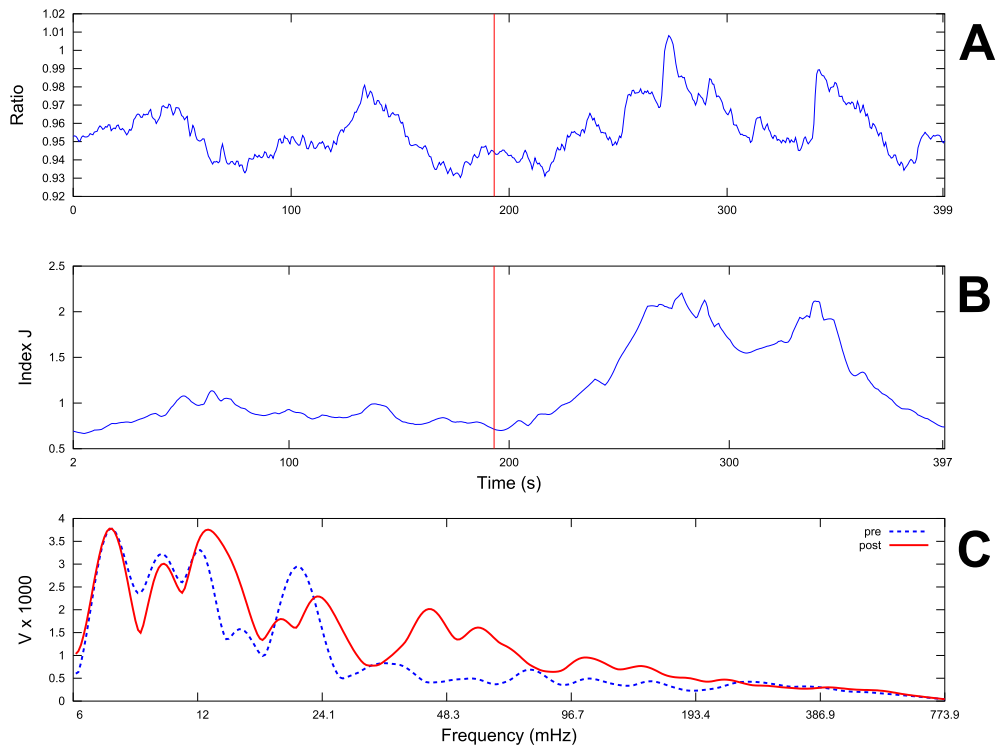


Figure 8: Third trace. **A:** oscillations in $[Ca^{2+}]_c$ observed in response to stimulation of a CG glial cells with 10 nM NAADP. **B:** time course of the index J . **C:** the dashed line represents the vector \mathbf{V}_1 , computed from the pre-stimulus signal, whereas the continuous line refers to \mathbf{V}_2 , corresponding to the post-stimulus signal.

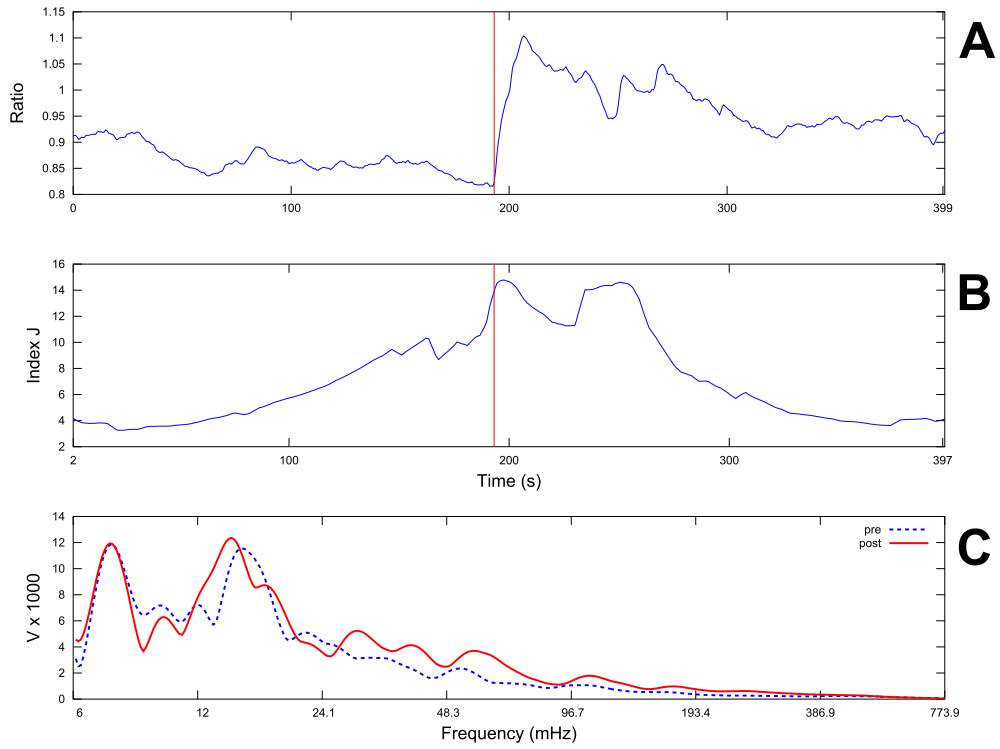


Figure 9: Fourth trace. **A:** oscillations in $[Ca^{2+}]_c$ observed in response to stimulation of a CG glial cells with 10 nM NAADP. **B:** time course of the index J . **C:** the dashed line represents the vector \mathbf{V}_1 , computed from the pre-stimulus signal, whereas the continuous line refers to \mathbf{V}_2 , corresponding to the post-stimulus signal.

387 The observation that changes in the frequency content span the same
 388 range in all four cells shown (Figs. 6, 7, 8, 9) can be formalized in a more
 389 objective quantification of the effect of the agonist, simply defining a new
 390 function:

$$R(\nu) = \frac{1}{N} \sum_{i=1}^N \left(\frac{V_2(\nu)}{V_1(\nu)} \right)_i, \quad (18)$$

391 where the sum runs over cells number: thus R is the mean ratio of post- to
 392 pre-treatment spectra.

393 The function R represents the average spectral distribution of the oscil-
 394 latory activity enhancement, following agonist administration. The function
 we obtained is clearly a non-flat distribution (Fig. 10). In particular it

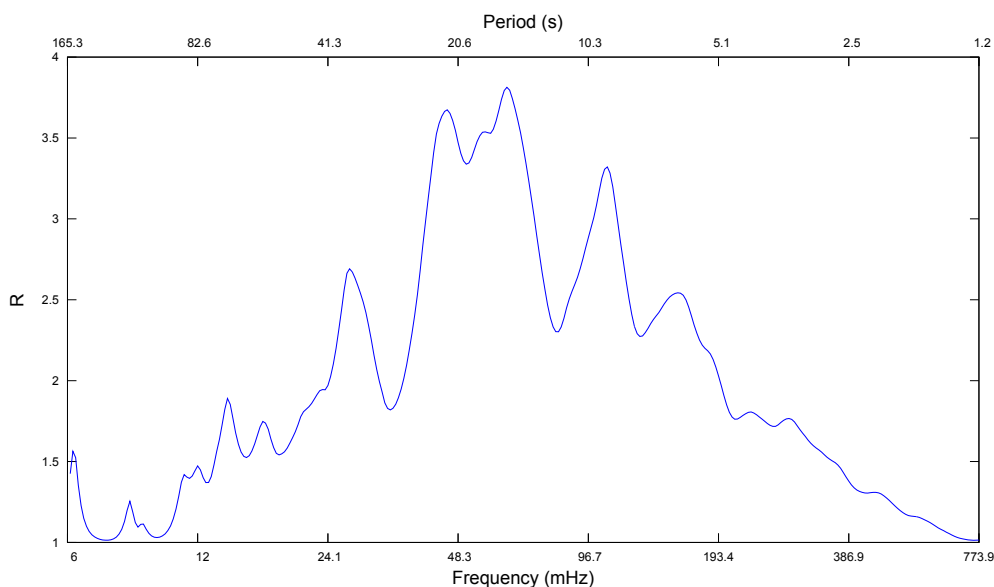


Figure 10: The function R as given by Eq. (18); here $N = 4$.

395 presents its highest values inside that same range of frequencies previously
 396 mentioned (24 – 193 mHz), with a peak centered on 50 mHz. Even if the
 397 number of cells used in this data analysis is small ($N = 4$), function (18)
 398 turns out to be able to discriminate the frequencies involved in cellular oscil-
 399 latory response, but is reasonable to think that this function would have been
 400 more smooth and more peaked if we had kept into account a larger number
 401 of traces. A step in this direction is presented in the following section.
 402

403 *4.1. Statistical validation*

404 It has been observed in section 3.1 that the ratio r_J provides a global
405 measure of the effect of the stimulus on the signal time course and that, in
406 particular, $r_J > 1$ should correspond to an enhancement of $[Ca^{2+}]_c$ oscilla-
407 tions and $0 < r_J < 1$ to an inhibition.

408 To provide a statistical validation of r_J values, we have considered a set
409 of 36 traces from 6 different experiments similar to those described above,
410 the only difference being that now CG glial cells were bathed in a Tyrode
411 standard solution and then stimulated with a higher dose of NAADP (1 μ M;
412 data not shown). For each trace the corresponding r_J was computed, thus
413 generating a sample $\{r_J\}$ whose histogram is shown in Fig. 11.A.

414 While it is clear that r_J is not normally distributed, as it could be expected
415 since its range is from 0 to $+\infty$, a distribution more closely resembling a
416 normal can be obtained by considering a transformation from r_J to $\log r_J$
417 (see Fig. 11.B). Indeed a Q-Q plot (Fig. 11.C) shows the data lying very
418 close to the bisector; a Shapiro-Wilk (SW) normality test gives $p = 0.639$,
419 much higher than the threshold for the rejection of normality hypothesis
420 $\alpha = 0.05$.

421 It follows that we can assume the distribution of r_J to be log-normal, and
422 this holds also for the sampling distribution obtained by application to our
423 sample of a bootstrap procedure with 10^6 iterations.

424 We have then computed the mean and corresponding confidence inter-
425 val (*CI*) for the original data and the bootstrap distribution, and both ap-
426 proaches lead to the same numerical results. In both cases $\bar{r}_J = 2.49$, and
427 $CI = [2.02; 3.04]$ is the 99% confidence interval; namely there is a probability
428 $p \geq 0.99$ that the true value of the index r_J is comprised between 2.02 and
429 3.04.

430 If r_J did not measure the effect of the stimulus on the oscillatory activity
431 of $[Ca^{2+}]_c$ time course any departure from $r_J = 1$ would be ascribed solely
432 to chance; since $r_J = 1$ is outside the 99% confidence interval we can reject
433 the null hypothesis that $r_J = 1$ is the true value of index r_J .

434 With this approach, therefore, we provide a statistical validation of a
435 significant difference between pre- and post-stimulus condition in a whole set
436 of data, that is to say that the results reflect the occurrence of a response of
437 the cell population to the stimulus.

438 For comparison we have computed the index J using W values of all
439 frequencies, and not just those corresponding to the maxima; the index com-
440 puted this way does not give better results, thus confirming our hypothesis

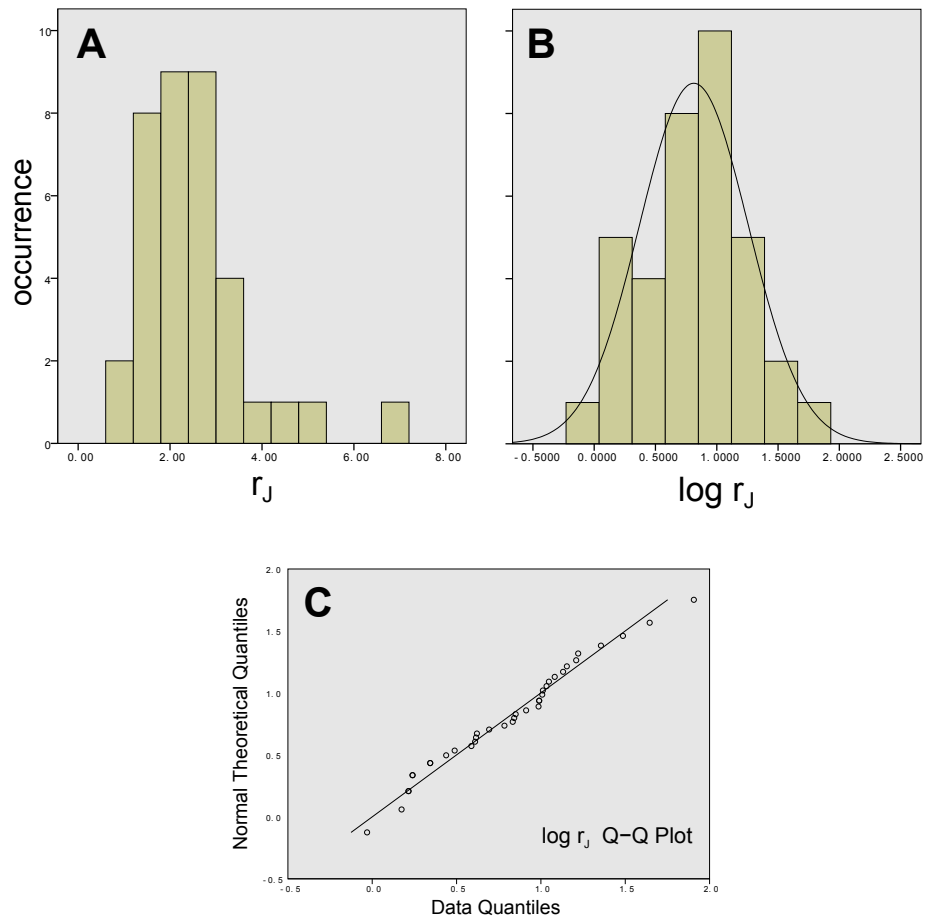


Figure 11: Statistical analysis. **A:** Histogram of r_J values computed from 36 different traces. The average of r_J is $\bar{r}_J = 2.49$. **B:** Histogram of the new variable $\log r_J$. **C:** Q-Q plot of the variable $\log r_J$.

441 that maxima contain most of the relevant information about the frequency
442 composition.

443 **5. Conclusion**

444 Wavelet analysis is a well known tool to study the properties of a signal
445 and to extract information about the temporal changes of its oscillatory
446 structure. However there are applications, such as analysis of changes in the
447 cytosolic free calcium concentration $[Ca^{2+}]_c$, that require to discriminate
448 between different patterns of signal activity either in space or in time. Here
449 an approach has been presented in which by separating time and frequency
450 domains, indices have been derived to characterize quantitatively changes
451 in the oscillatory behavior of $[Ca^{2+}]_c$ with respect to different experimental
452 conditions, in particular pre- and post-stimulus conditions. This approach
453 has been tested on a set of experimental recordings showing heterogeneous
454 patterns of activation, and it has been proved to be able to discern subtle
455 differences between them.

456 In particular the procedure described here represents a general method
457 that allows a rigorous and automated characterization of both cellular spon-
458 taneous activity and effects of agonists in terms of oscillatory behaviors. This
459 approach has been used here for discriminating between different patterns in
460 time, but it could be highly useful in different contexts, such as in analyzing
461 spatial differences in signals recorded from subdomains of the same cell.

462 **6. Acknowledgments**

463 We thank Prof. A. Genazzani for the gift of NAADP used in the experi-
464 ments.

465 **References**

- 466 Antonini M, Barlaud M, Mathieu P, Daubechies I. Image coding using
467 wavelet transforms. IEEE Trans Image Process 1992;1:205–20.
- 468 Bernascone S, Erriquez J, Ferraro M, Genazzani AA, Distasi C. Novel adeno-
469 sine and cAMP signalling pathways in migrating glial cells. Cell Calcium
470 2010;48:83–90.

- 471 Billington RA, Bellomo EA, Floriddia EM, Erriquez J, Distasi C, Genazzani
472 AA. A transport mechanism for NAADP in a rat basophilic cell line.
473 FASEB J 2006;20:521–3.
- 474 Billington RA, Genazzani AA. Characterization of NAADP(+) binding in
475 sea urchin eggs. Biochem Biophys Res Commun 2000;276:112–6.
- 476 Bussow R. An algorithm for the continuous Morlet wavelet transform. Mech
477 Syst Signal Process 2007;21:2970–9.
- 478 Constantin S, Caligioni CS, Stojilkovic S, Wray S. Kisspeptin-10 facilitates
479 a plasma membrane-driven calcium oscillator in gonadotropin-releasing
480 hormone-1 neurons. Endocrinology 2009;150:1400–12.
- 481 Daubechies I. Ten lectures on wavelets. Philadelphia, Penn: Society for
482 Industrial and Applied Mathematics, 1992.
- 483 Distasi C, Torre M, Antoniotti S, Munaron L, Lovisolo D. Neuronal survival
484 and calcium influx induced by basic fibroblast growth factor in chick ciliary
485 ganglion neurons. Eur J Neurosci 1998;10:2276–86.
- 486 Eaton JW, Bateman D, Hauberg S. GNU Octave manual. UK: Network
487 Theory Ltd, 2008.
- 488 Frey N, McKinsey TA, Olson EN. Decoding calcium signals involved in
489 cardiac growth and function. Nat Med 2000;6:1221–7.
- 490 Genazzani AA, Billington RA. NAADP: an atypical Ca²⁺-release messen-
491 ger? Trends Pharmacol Sci 2002;23:165–7.
- 492 Goldberg JH, Yuste R. Space matters: local and global dendritic Ca²⁺ com-
493 partmentalization in cortical interneurons. Trends Neurosci 2005;28:158–
494 67.
- 495 Gorbunova YV, Spitzer NC. Dynamic interactions of cyclic AMP transients
496 and spontaneous Ca(2+) spikes. Nature 2002;418:93–6.
- 497 Goupillaud P, Grossman A, Morlet J. Cycle-Octave and related transforms
498 in seismic signal analysis. Geoprospection 1984;23:85–102.
- 499 Lokenath D. Brief historical introduction to wavelet transforms. Int J Math
500 Educ Sci Technol 1998;29:677–88.

- 501 Mallat S. A wavelet tour of signal processing. San Diego, Ca: Academic
502 Press, 1999.
- 503 Oike M, Droogmans G, Nilius B. Amplitude modulation of Ca²⁺ signals
504 induced by histamine in human endothelial cells. *Biochim Biophys Acta*
505 1994;1222:287–91.
- 506 Prank K, Gabbiani F, Brabant G. Coding efficiency and information rates
507 in transmembrane signaling. *Biosystems* 2000;1-3:15–22.
- 508 Raymond CR, Redman SJ. Spatial segregation of neuronal calcium signals
509 encodes different forms of LTP in rat hippocampus. *J Physiol* 2006;570:97–
510 111.
- 511 Suzuki N, Takahata M, Sato K. Oscillatory current responses of olfactory
512 receptor neurons to odorants and computer simulation based on a cyclic
513 AMP transduction model. *Chem Senses* 2002;27:789–801.
- 514 Torrence C, Compo GP. A practical guide to wavelet analysis. *Bull Am*
515 *Meteorol Soc* 1998;79:61–78.
- 516 Uhlén P. Spectral analysis of calcium oscillations. *Sci STKE* 2004;258:1–12.
- 517 Uhlén P, Fritz N. Biochemistry of calcium oscillations. *Biochem Biophys*
518 *Res Commun* 2010;396:28–32.
- 519 Wegner F, Both M, Fink RH. Automated detection of elementary calcium
520 release events using the a trous wavelet transform. *Biophys J* 2006;90:2151–
521 63.
- 522 Wen Z, Zheng JQ. Directional guidance of nerve growth cones. *Curr Opin*
523 *Neurobiol* 2006;16:52–8.

524 **List of Figures**

525	1	Real and imaginary parts of the Morlet mother wavelet, as	
526		given by Eq. (4).	5
527	2	A: oscillations in $[Ca^{2+}]_c$ observed in response to stimulation	
528		of a chick CG glial cells with 10 nM NAADP. A vertical line	
529		marks the starting time of perfusion with the agonist. B:	
530		$ W(t, \nu) $: amplitude of the wavelet transform as a function of	
531		time and frequency.	7
532	3	Projections. The central box shows the modulus of the wavelet	
533		transform. In the insets: on the left the power spectrum as	
534		defined in Eq. (7) and on the top the energy density (see Eq.	
535		(6)).	8
536	4	Fourier and wavelet spectra superimposed in a log-log coordi-	
537		nates: the wavelet power spectrum results in a smoother ver-	
538		sion of the Fourier spectrum, overemphasizing high frequencies.	9
539	5	Time course of the index J , computed applying Eq. (9) to the	
540		modulus of the wavelet transform shown in Fig. 2.	10
541	6	Vector analysis. The dashed line represents the vector \mathbf{V}_1 ,	
542		computed from the pre-stimulus signal, whereas the continu-	
543		ous line refers to \mathbf{V}_2 , corresponding to the post-stimulus signal.	14
544	7	Second trace. A: oscillations in $[Ca^{2+}]_c$ observed in response	
545		to stimulation of a CG glial cells with 10 nM NAADP. B:	
546		time course of the index J . C: the dashed line represents the	
547		vector \mathbf{V}_1 , computed from the pre-stimulus signal, whereas	
548		the continuous line refers to \mathbf{V}_2 , corresponding to the post-	
549		stimulus signal.	18
550	8	Third trace. A: oscillations in $[Ca^{2+}]_c$ observed in response	
551		to stimulation of a CG glial cells with 10 nM NAADP. B:	
552		time course of the index J . C: the dashed line represents the	
553		vector \mathbf{V}_1 , computed from the pre-stimulus signal, whereas	
554		the continuous line refers to \mathbf{V}_2 , corresponding to the post-	
555		stimulus signal.	19

556	9	Fourth trace. A: oscillations in $[\text{Ca}^{2+}]_c$ observed in response	
557		to stimulation of a CG glial cells with 10 nM NAADP. B:	
558		time course of the index J . C: the dashed line represents the	
559		vector \mathbf{V}_1 , computed from the pre-stimulus signal, whereas	
560		the continuous line refers to \mathbf{V}_2 , corresponding to the post-	
561		stimulus signal.	20
562	10	The function R as given by Eq. (18); here $N = 4$	21
563	11	Statistical analysis. A: Histogram of r_J values computed from	
564		36 different traces. The average of r_J is $\bar{r}_J = 2.49$. B: His-	
565		togram of the new variable $\log r_J$. C: Q-Q plot of the variable	
566		$\log r_J$	23